Comparative Analysis of Two-Coil and Three-Coil Structures for Wireless Power Transfer

Jian Zhang, *Student Member, IEEE*, Xinmei Yuan, *Member, IEEE*,
Chuang Wang, *Student Member, IEEE*, and Yang He

***Abstract*—With the development of electric vehicles and consumer electronics, wireless power transfer (WPT) is becoming a popular technology. Recently, magnetic resonant coupling has been considered to be the most effective and attractive WPT approach, and the two-coil structure is the most widely used for magnetic resonant coupling. It has been recently reported that the system's energy efficiency can be improved by a three-coil structure. In this paper, the three-coil structure is compared with the two-coil structure based on circuit theory. Simplified circuit models of the two- and three-coil structures are proposed to give a more intuitive and comprehensive analysis of the energy efficiency differences between the two structures. With the simplified model, the condition for a three-coil structure obtaining higher energy efficiency over its two-coil counterpart is derived, and the analysis shows that the WPT system with higher energy efficiency within a wider range of loads can be achieved by properly designed three-coil systems. Additionally, it also shows that the three-coil system has the significant advantage of reducing the current stress and the electromagnetic field emission that is caused by misalignments. The theoretical analysis is confirmed by both simulation and experimental results.**

***Index Terms*—Energy efficiency, load variation, misalignment, resonators, wireless power transfer.**

I. Introduction

With the advantages of safety and convenience, wireless power transfer (WPT) technology shows great potential for applications in electric vehicles [1]–[6] and consumer electronics [7], [8]. Magnetic resonant coupling is currently considered to be the most effective and attractive WPT approach.

The primary design objectives of magnetic resonant coupling-based WPT systems are to increase the power transfer capacity and improve the energy efficiency. Basically, the power transfer capacity is decided by the resonant frequency, coupling coefficient and load impedance of the system, and the energy efficiency is affected by losses from power electronics, the iron core, and equivalent series resistances (ESRs) of resonators. In general, impedance matching is most widely used to maximize the transfer power. Impedance matching is a common practice in many radio frequency circuit designs, which occurs when the input resistance equals the internal resistance of the power source, but the overall energy efficiency of the impedance matching WPT system is limited to below 50% [9]–[11]. To improve the transfer energy efficiency, soft switching, GaN, or SiC power devices are adopted to reduce the losses in the power electronics; using lower resonant frequencies is another approach to lowering the losses of power electronics and the iron core; and Litz wires and film capacitors are chosen for their low ESR properties.

An additional control variable or system component is needed to further improve the WPT system's characteristics. Maximum energy efficiency tracking is realized by adjusting the input voltage or/and the output voltage using power converters [12]–[15]. Relays are designed to select capacitors and/or coils to be connected to the resonant circuits to improve the energy efficiency against system parameter variations [16]–[18]. By tuning the operating frequency, the power transfer capacity can be maximized in the over-coupled region to reduce the influence of the frequency splitting phenomena [19], [20]. Typical additional components are additional coils in the power transfer path. The source coil (also called driving coil) and load coil in the four-coil structure are the most widely used components to improve the power transfer capacity, because impedance matching can be achieved by tuning the parameters of these additional coils [21], [22]. With the relay resonators (also referred to as domino resonator, intermediate coils, or repeater) placed at optimum positions, the overall WPT distance and energy efficiency can be substantially increased [23]–[27]. The limitation of this structure is that relay resonators require positions at which they are to be fixed, which should be between the transmitter coil and receiving coil.

A three-coil structure is a special case of having an additional component for a WPT system. An additional resonator is added to either the transmitter or the receiver, which can be placed on the same plane as the transmitter/receiving coil or only adjacent to the transmitter/receiving coil. The additional resonator in a three-coil structure is different from the relay resonator because it does not use the space between the transmitter coil and receiving coil. For example, in the electric vehicle WPT system, an additional source coil is added to the transmitter, as shown in Fig. 1, the transmission distance (distance between transmitter coil and receiving coil) is fixed, and relay resonators are not allowed between the transmitter coil and receiving coil. However, the additional source coil can also be beneficial for the WPT efficiency.

In three-coil structures, the additional coil placed in the transmitter or receiver is different. If the additional coil is placed in the receiver, the load impedance can be reflected to obtain an

Manuscript received November 4, 2015; revised January 2, 2016; accepted February 3, 2016. Date of publication February 8, 2016; date of current version September 16, 2016. This paper is an expanded version from the *IEEE MTT-S International Wireless Symposium*, Shenzhen, China, Mar. 2015. Recommended for publication by Associate Editor O. Lucia.

The authors are with the State Key Laboratory of Automobile Simulation and Control, Jilin University, Changchun 130025, China (e-mail: 506389607@qq.com; yuan@jlu.edu.cn; 1158671825@qq.com; 731655017@qq.com).

Color versions of one or more of the figures in this paper are available online at http://ieeexplore.ieee.org.

Digital Object Identifier 10.1109/TPEL.2016.2526780

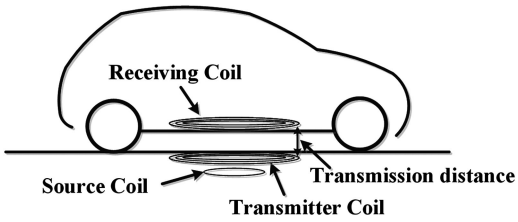

Fig. 1. Example of the three-coil structure used for electric vehicle wireless charging.

optimal value by adjusting the coupling coefficient of the additional coil and receiving coil, which achieves both arbitrary load impedance to the optimal value and high power delivered to the load. An in-depth comparative analysis of this structure has been given in [28]. In contrast, the additional coil has been placed in the transmitter in recent years; it is found that this structure can further improve the energy efficiency of the WPT system [29]–[32]. The physical background of the latter structure is that the source impedance can be converted to be smaller by the additional coil or the input impedance can be converted to be larger, and therefore, the total energy efficiency of the system is increased. In this paper, only the latter structure is discussed.

In addition to the energy efficiency optimization, the design of the WPT system also requires consideration of the tolerances of system parameter variations, the load variations, and the misalignment and electromagnetic field (EMF) emission [33], [34]. Most previous studies of the three-coil system focus only on the system's energy efficiency; the energy efficiency tolerances of the transfer distance variation, the load variation, and coil misalignments have been scarcely discussed. A primary reason for the lack of these discussions is that the expression of the system efficiency is too complex to analyze and the numerical and experimental results are difficult to generalize. In [29], the energy efficiency and EMF emission characteristics of the three-coil structure is discussed and experimentally tested, but the conditions under which the three-coil structure obtains energy efficiency benefits were not given, and the conclusions have not been strictly proven. Additionally, in [29], limited by the mechanical structure, the distance between the source coil and transmitter coil cannot be reduced to small values, but a strong coupling of the source coil and transmitter coil is found to be a very important operating condition for the three-coil structures. In this paper, to provide in depth insight into the system characteristics of the three-coil structure, simplified circuit models are proposed to compare the three-coil structure and the two-coil structure. Based on the simplified models, the conditions under which the three-coil structure obtains a higher energy efficiency than its two-coil counterpart are derived, and it is proven that the efficiency stiffness against the load variation around the maximum efficiency point can be improved by the three-coil structure. Finally, the trends in the variations of the currents of the two structures when the coils are misaligned are derived. It is found that the three-coil system shows great benefit in preventing the current stress and EMF emissions that are induced by coil misalignments. With our experimental setup, the distance between the source coil and transmitter coil can be

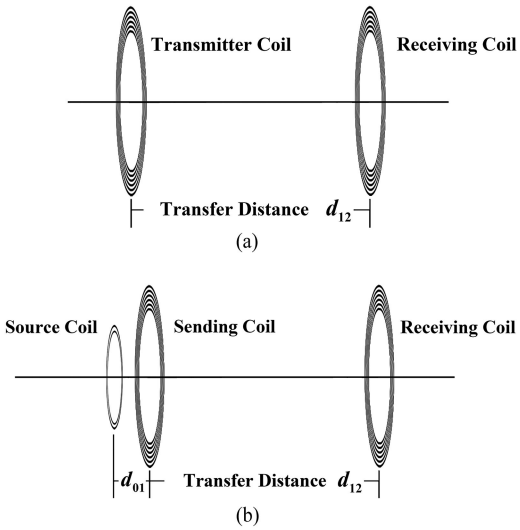

Fig. 2. Structures of two-coil and three-coil systems. (a) Two-coil system. (b) Three-coil system.

continuously adjusted from 0 to 30 mm, and the misalignments of the transmitter coil and receiving coil can be continuously adjusted from 0 to 40 mm. Therefore, the characteristics of the two- and three-coil structures can be extensively tested, and both the simulation and experimental results are provided to confirm key analytical results.

This paper is organized as follows. In Section II, the basic circuit models of the two- and three-coil systems are described. The analysis and comparison of the two- and three-coil structures are presented based on simplified circuit models in Section III. The results of the analysis are simulated and experimentally validated in Section IV. Finally, Section V contains some concluding remarks.

II. Circuit Model

The common two- and three-coil structures for WPT systems are illustrated in Fig. 2. The only difference between the two structures is the additional source coil of the three-coil system in Fig. 2(b). The source coil is always placed on the same plane as the transmitter coil, but for general analysis, the distance of d_{01} is used to adjust the mutual inductance between the source coil and transmitter coil. For midrange coupling conditions, it has been proven that both coupled-mode theory and circuit theory basically result in the same set of equations in the steady state and that either method can be applied [35]–[37]. Circuit theory is used in this paper. The equivalent circuits of the two structures are shown in Fig. 3, where the subscripts 0, 1, and 2 denote the source coil, transmitter coil, and receiving coil, respectively, L is the inductance of the coil, C is the resonant capacitance series connected to the coils, M is the mutual inductance, R is the ESR in the circuit, $\mathbf{U}$ is the voltage phasor, $\mathbf{I}$ is the current phasor, R_L is the load resistance, P_i is the input power, P_o is the output power, R_s is the internal resistance of the power source, and $R_{\rm in}$ is the input impedance of the circuit at the resonance frequency

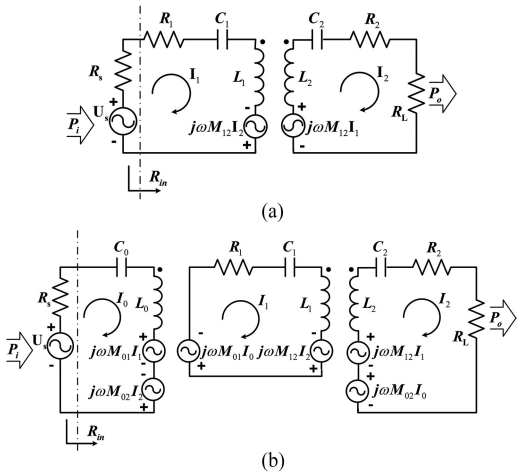

Fig. 3. Equivalent circuits of two-coil and three-coil systems. (a) Two-coil system. (b) Three-coil system.

ω_0. Because the size of the source coil is small, R_0 is assumed to be negligible compared with R_s.

The circuit equations of the two-coil structure at the resonance frequency are the following:

$$\mathbf{U}_s = (R_s + R_1)\mathbf{I}_1 - j\omega_0 M_{12}\mathbf{I}_2 \tag{1}$$

$$j\omega_0 M_{12}\mathbf{I}_1 = (R_2 + R_L)\mathbf{I}_2. \tag{2}$$

Using (2), the current of the receiving coil can be expressed as

$$\mathbf{I}_2 = \frac{j\omega_0 M_{12}}{R_2 + R_L}\mathbf{I}_1. \tag{3}$$

Substituting (3) into (1), the input power can be calculated by

$$P_i^{2c} = \mathbf{Re}\left(\mathbf{U}_s\mathbf{I}_1\right) = \left(R_s + R_1 + \frac{\omega_0^2 M_{12}^2}{R_2 + R_L}\right)\left|\mathbf{I}_1\right|^2. \tag{4}$$

The output power can be calculated by

$$P_o^{2c} = R_L\left|\mathbf{I}_2\right|^2 = R_L\frac{\omega_0^2 M_{12}^2}{\left(R_2 + R_L\right)^2}\left|\mathbf{I}_1\right|^2. \tag{5}$$

The power transfer efficiency can be obtained as

$$\eta_{2c} = \frac{P_o^{2c}}{P_i^{2c}} = \frac{1}{a_{2c}R_L + \frac{b_{2c}}{R_L} + c_{2c}} \tag{6}$$

where subscript $2c$ denotes the two-coil system, and a, b, and c are parameters that are defined in Table I. From (6), the optimal load condition for the maximum energy efficiency can be expressed as

$$R_L^{\mathrm{opt}_{2c}} = \sqrt{\frac{b_{2c}}{a_{2c}}}. \tag{7}$$

Similar to the two-coil structure, the circuit equations of the three-coil structure at the resonance frequency are

$$\mathbf{U}_s = R_s\mathbf{I}_0 - j\omega_0 M_{01}\mathbf{I}_1 + j\omega_0 M_{02}\mathbf{I}_2 \tag{8}$$

$$-j\omega_0 M_{01}\mathbf{I}_0 = R_1\mathbf{I}_1 - j\omega_0 M_{12}\mathbf{I}_2 \tag{9}$$

$$j\omega_0 M_{12}\mathbf{I}_1 + j\omega_0 M_{02}\mathbf{I}_0 = (R_2 + R_L)\mathbf{I}_2. \tag{10}$$

The currents of the transmitter coil and receiving coil can be expressed as

$$\mathbf{I}_1 = \frac{-j\omega_0 M_{01}\left(R_2 + R_L\right) - \omega_0^2 M_{02}M_{12}}{R_1\left(R_2 + R_L\right) + \omega_0^2 M_{12}^2}\mathbf{I}_0 \tag{11}$$

$$\mathbf{I}_2 = \frac{\omega_0^2 M_{01}M_{12} + j\omega_0 M_{02}R_1}{R_1\left(R_2 + R_L\right) + \omega_0^2 M_{12}^2}\mathbf{I}_0. \tag{12}$$

In (11) and (12), using the parameters of our experimental setup in Table III, the terms with M_{02} are approximately two orders of magnitude smaller than the other terms in the numerators; therefore, the effect of M_{02} is neglected in this study, and (11) and (12) are simplified as

$$\mathbf{I}_1 = \frac{-j\omega_0 M_{01}\left(R_2 + R_L\right)}{R_1\left(R_2 + R_L\right) + \omega_0^2 M_{12}^2}\mathbf{I}_0 \tag{13}$$

$$\mathbf{I}_2 = \frac{\omega_0^2 M_{01}M_{12}}{R_1\left(R_2 + R_L\right) + \omega_0^2 M_{12}^2}\mathbf{I}_0. \tag{14}$$

However, because M_{02} brings an imaginary part into (12), the resonant characteristics of the WPT system are changed. It has been reported that the cross-coupling effects of nonadjacent resonators would cause the maximum efficiency operation to shift away slightly from the resonance frequency in domino-resonator systems [24], and the source coil could induce a bifurcation phenomenon in the three-coil system [30]; therefore, if M_{02} cannot be neglected, then the operating frequency is an important factor for the three-coil system.

Substituting (13) into (8), the input power can be calculated by

$$P_i^{3c} = \mathbf{Re}\left(\mathbf{U}_s\mathbf{I}_0\right) = \left(R_s + \frac{\omega_0^2 M_{01}^2\left(R_2 + R_L\right)}{R_1\left(R_2 + R_L\right) + \omega_0^2 M_{12}^2}\right)\left|\mathbf{I}_0\right|^2. \tag{15}$$

Using (14), the output power can be calculated by

$$P_o^{3c} = R_L\left|\mathbf{I}_2\right|^2 = R_L\frac{\omega_0^4 M_{01}^2 M_{12}^2}{\left(R_1\left(R_2 + R_L\right) + \omega_0^2 M_{12}^2\right)^2}\left|\mathbf{I}_0\right|^2. \tag{16}$$

Then, the power transfer efficiency of the three-coil system can be derived from (15) and (16) as

$$\eta_{3c} = \frac{P_o^{3c}}{P_i^{3c}} = \frac{1}{a_{3c}R_L + \frac{b_{3c}}{R_L} + c_{3c}} \tag{17}$$

where subscript $3c$ denotes the three-coil system, and a, b, and c are parameters that are defined in Table I. Similarly, the optimal load condition for maximum energy efficiency operation of the three-coil system is

$$R_L^{\mathrm{opt}_{3c}} = \sqrt{\frac{b_{3c}}{a_{3c}}}. \tag{18}$$

Fortunately, (17) and (18) have the same form as (6) and (7), which shows that the additional source coil only increases the complexity of the parameter expressions of a, b, and c but does not increase the order of the energy efficiency expressions. Therefore, the analysis of the different coil structures can simply focus on the variations of these parameters.

TABLE I
EXPRESSIONS OF THE TWO- AND THREE-COIL SYSTEMS AT THE RESONANCE FREQUENCY

	Two-coil system (2c)	Three-coil system (3c)
R_{in}	$R_1 + \dfrac{\omega_0^2 M_{12}^2}{R_2 + R_L}$	$\dfrac{\omega_0^2 M_{01}^2 (R_2 + R_L)}{R_1 (R_2 + R_L) + \omega_0^2 M_{12}^2}$
a	$\dfrac{R_s + R_1}{\omega_0^2 M_{12}^2}$	$\dfrac{R_1 (R_s R_1 + \omega_0^2 M_{01}^2)}{\omega_0^4 M_{01}^2 M_{12}^2}$
b	$\left(\dfrac{(R_s + R_1) R_2}{\omega_0^2 M_{12}^2} + 1 \right) R_2$	$\dfrac{(R_1 R_2 + \omega_0^2 M_{12}^2)(R_s R_1 R_2 + \omega_0^2 M_{12}^2 R_s + \omega_0^2 M_{01}^2 R_2)}{\omega_0^4 M_{01}^2 M_{12}^2}$
c	$\dfrac{2(R_s + R_1) R_2}{\omega_0^2 M_{12}^2} + 1$	$\dfrac{(R_s R_1 + \omega_0^2 M_{01}^2)(R_1 R_2 + \omega_0^2 M_{12}^2) + R_1 (R_s R_1 R_2 + \omega_0^2 M_{12}^2 R_s + \omega_0^2 M_{01}^2 R_2)}{\omega_0^4 M_{01}^2 M_{12}^2}$
R_L^{opt}	$\sqrt{\dfrac{R_2}{R_s + R_1} \left((R_s + R_1) R_2 + \omega_0^2 M_{12}^2 \right)}$	$\sqrt{\dfrac{(R_1 R_2 + \omega_0^2 M_{12}^2)(R_s R_1 R_2 + \omega_0^2 M_{12}^2 R_s + \omega_0^2 M_{01}^2 R_2)}{R_1 (R_s R_1 + \omega_0^2 M_{01}^2)}}$

III. CIRCUIT ANALYSIS

The expressions in Table I are complex and very difficult to understand. Consequently, a simplification method for the expressions in Table I is proposed in this section. Based on the simplified expressions, the essential differences between the two- and three-coil structures are discussed.

A. Simplification

When the source internal resistance $R_s = 0$, the expressions of a, b, c, and R_L^{opt} in the different columns in Table I reduce to the same expressions and, thus, the differences between the energy efficiencies of the two- and three-coil systems come from the internal resistance of the power source, which indicates that the differences in the energy efficiencies between the two- and three-coil systems become more obvious as the source impedance increases, and this conclusion is consistent with previous studies [31], [32].

When R_s is not negligible, because the ESRs of the coils (R_1 and R_2) and the internal resistance of the power source (R_s) are relatively small, the following relationship is assumed:

$$R_s R_1 \ll \omega_0^2 M_{01}^2 \tag{19}$$

$$R_1 R_2 \ll \omega_0^2 M_{12}^2 \tag{20}$$

$$R_s R_2 \ll \omega_0^2 M_{12}^2. \tag{21}$$

Because R_2 is series connected with R_L and the energy is expected to be transferred to R_L, we assume

$$R_2 \ll R_L. \tag{22}$$

Then, the expressions in Table I can be simplified to the expressions in Table II. Compared with the expressions in Table I, the simplified expressions are much more clear and intrinsic. For example, it is difficult to compare the energy efficiency expression parameters in Table I, especially for the three-coil system, but with our simplification, the following inequalities can be easily obtained

TABLE II
SIMPLIFIED EXPRESSIONS OF THE TWO- AND THREE-COIL SYSTEM AT THE RESONANCE FREQUENCY

	Two-coil system (2c)	Three-coil system (3c)
R_{in}	$R_1 + \dfrac{\omega_0^2 M_{12}^2}{R_L}$	$\dfrac{M_{01}^2}{\frac{R_1}{\omega_0^2} + \frac{M_{12}^2}{R_L}}$
a	$\dfrac{R_s + R_1}{\omega_0^2 M_{12}^2}$	$\dfrac{R_1}{\omega_0^2 M_{12}^2}$
b	R_2	$\dfrac{M_{12}^2 R_s}{M_{01}^2} + R_2$
c	1	1
R_L^{opt}	$\omega_0 M_{12} \sqrt{\dfrac{R_2}{R_s + R_1}}$	$\omega_0 M_{12} \sqrt{\dfrac{1}{R_1} \left(R_2 + \dfrac{M_{12}^2}{M_{01}^2} R_s \right)}$

$$a_{2c} > a_{3c} \tag{23}$$

$$b_{2c} < a_{3c} \tag{24}$$

$$c_{2c} \simeq c_{3c} \simeq 1 \tag{25}$$

and the differences in the above parameters for the two structures are caused by R_s.

To verify the simplification method, the efficiency characteristics and the input impedance of the two- and three-coil systems are calculated by MATLAB using the expressions in Tables I and II, respectively. The values of the parameters used in the simulation are from our experimental system, which are shown in Table III. The results of the simulation are presented in Fig. 4. In these figures, both the energy efficiency and the input impedance of the simplified model match the trends of the original model well, but there is a 5% error approximately that is caused by the simplification. Nevertheless, the shapes of the simplified curves are not changed, and the shifting of the simplified curves of the two- and three-coil systems are approximately

TABLE III
PARAMETERS OF THE COILS USED IN EXPERIMENTS

R_1	0.4 Ω	L_1	16.2 μH	C_1	3.34 nF	M_{12}(62 mm)	0.81 μH
R_2	0.8 Ω	L_2	16.2 μH	C_2	3.34 nF	M_{01}(0 mm)	1.50 μH
R_s	0.32 Ω	L_0	1.53 μH	C_0	35.4 nF	M_{02}(0 mm)	0.094 μH

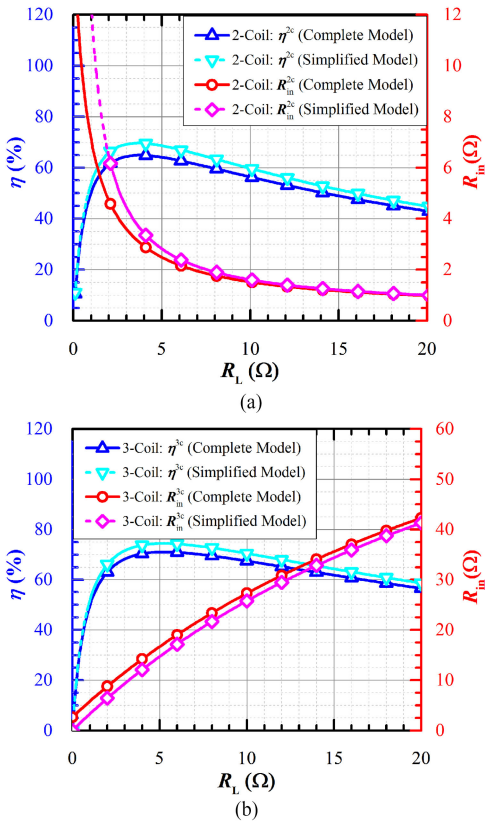

Fig. 4. Simulated energy efficiencies and input impedances of the two- and three-coil systems using original and simplified models. (a) Two-coil system. (b) Three-coil system.

the same; therefore, it is feasible to use the simplified models to obtain the dominant characteristics and the design guidelines of the two- and three-coil systems. Thereafter, the original complete circuit model can be used for detailed circuit simulation and optimization. In general, the ESRs and the source internal resistance of the WPT system become relatively small while the transfer power increases and, thus, the errors of the simplified model become smaller in higher power systems.

B. Maximum Energy Efficiency

It has been reported that specified conditions are required for the efficiency of the three-coil system to be higher than that of the two-coil system [31], [32], but those conditions are derived from complete system equations; therefore, they are rather complex and difficult to apply in practical system design. With the simplified energy efficiency expressions, a much simpler condition can be derived. Substituting (7) into (6), the maximum energy efficiency of the two- or three-coil systems can be expressed as

$$\eta^{\max} = \frac{1}{2\sqrt{ab}+c}. \tag{26}$$

Using the expressions in Table II, we have

$$\eta_{2c}^{\max} \simeq \frac{1}{2\sqrt{\frac{R_s+R_1}{\omega_0^2 M_{12}^2}R_2}+1} \tag{27}$$

$$\eta_{3c}^{\max} \simeq \frac{1}{2\sqrt{\frac{M_{12}^2 R_s + M_{01}^2 R_2}{\omega^2 M_{12}^2 M_{01}^2}R_1}+1}. \tag{28}$$

If the maximum efficiency of the three-coil system is higher than that of the two-coil system, the energy efficiencies can be expressed as

$$\eta_{3c}^{\max} > \eta_{2c}^{\max}. \tag{29}$$

Substituting (27) and (28) into (29), the specified condition required for the efficiency of the three-coil system to be higher than its two-coil counterpart can be derived as

$$M_{01}^2 R_2 > M_{12}^2 R_1. \tag{30}$$

This inequality indicates that the three-coil system improves the maximum energy efficiency when the source coil is close enough to the transmitter coil and/or the transmitter coil and receiving coil are weakly coupled. This conclusion is consistent with previous studies [31], [32], [38], but it is much simpler and easier to apply. Using (30), with estimated ESRs, using the mutual inductances of the coils and using the energy transfer distance requirement, it is possible to decide whether the three-coil structure has an advantage over its two-coil counterpart. Equation (30) is easy to satisfy in general practice because M_{01} can be increased by placing the source coil close to or on the same plane as the transmitter coil; at the same time, the equivalent resistance of the rectifier makes R_2 larger than R_1. To verify the feasibility of the proposed condition of inequality (30), the maximum energy efficiencies of the two- and three-coil systems with parameter variations are compared. It is very difficult to find the analytical solution of the complete model using the expressions in Table I; therefore, numerical solutions of the maximum energy efficiencies with the M_{12} and M_{01} variations are calculated in MATLAB, and the ratios of $(M_{01}^2 R_2)/(M_{12}^2 R_1)$ are set to be from 0.2 to 1.8 by different mutual inductances. The simulation results are shown in Fig. 5. The simulation results show that when M_{12} increases, the maximum energy efficiency of the two-coil system increases faster than that of the three-coil system and becomes larger than its three-coil counterpart when $(M_{01}^2 R_2)/(M_{12}^2 R_1) > 1$. When M_{01} decreases, the maximum energy efficiency of the three-coil system decreases, but the energy efficiency of the two-coil system stays constant and, consequently, becomes larger compared with the three-coil system when $(M_{01}^2 R_2)/(M_{12}^2 R_1) > 1$. A most important feature in these results is that the critical conditions of the efficiency of the two- and three-coil systems are very close, approximately $(M_{12}^2 R_1)/(M_{01}^2 R_2) = 1$, which shows the feasibility of the proposed condition of inequality (30).

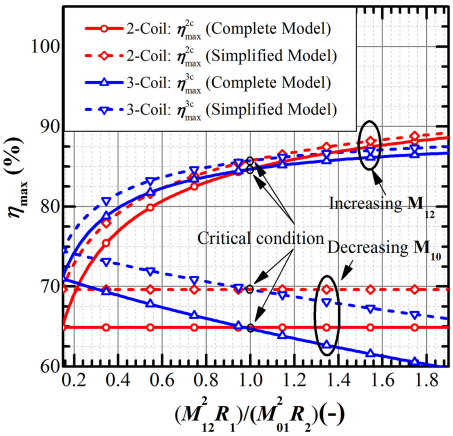

Fig. 5. Comparison of maximum energy efficiency with parameter variation.

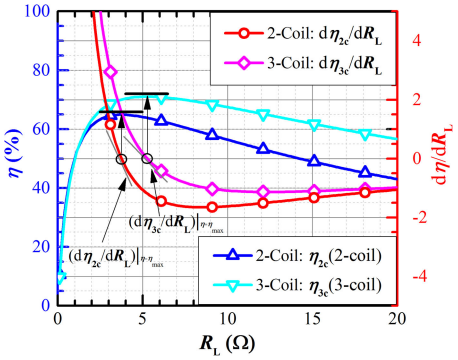

Fig. 6. Simulation results of the energy efficiencies and the derivatives of the energy efficiency.

C. Energy Efficiency Stiffness

Considering the tolerance of the system, the stiffness of the energy efficiency against the load variation is also compared. Because the energy efficiency expressions of the two- and three-coil systems are in the same form, the partial derivative of the efficiency with respect to the load resistance of the two structures can be derived as

$$\frac{\partial \eta}{\partial R_L} = -\frac{1}{\left(aR_L + \frac{b}{R_L} + c\right)^2}\left(a - \frac{b}{R_L^2}\right). \tag{31}$$

The maximum energy efficiency is achieved when $\partial\eta/\partial R_L = 0$ in the both two- and three-coil structures and, therefore, the second-order partial derivative of the energy efficiency at $\partial\eta/\partial R_L = 0$ is calculated

$$\left.\frac{\partial^2 \eta}{\partial R_L^2}\right|_{\frac{\partial \eta}{\partial R_L}=0} = \left.-\frac{2b}{R_L^3\left(aR_L + \frac{b}{R_L} + c\right)^2}\right|_{R_L=\sqrt{\frac{b}{a}}} \tag{32}$$

$$= -2\frac{a}{b}\frac{\sqrt{ab}}{\left(2\sqrt{ab} + c\right)^2}. \tag{33}$$

A comparison of the second-order partial derivative of the energy efficiency of the two structures around the maximum efficiency points yields

$$\frac{\left.\frac{\partial^2 \eta_{2c}}{\partial R_L^2}\right|_{\frac{\partial \eta_{2c}}{\partial R_L}=0}}{\left.\frac{\partial^2 \eta_{3c}}{\partial R_L^2}\right|_{\frac{\partial \eta_{3c}}{\partial R_L}=0}} = \left(\frac{a_{2c}b_{3c}}{a_{3c}b_{2c}}\right)\left(\frac{4\sqrt{a_{3c}b_{3c}} + \frac{c^2}{\sqrt{a_{3c}b_{3c}}} + 4c}{4\sqrt{a_{2c}b_{2c}} + \frac{c^2}{\sqrt{a_{2c}b_{2c}}} + 4c}\right). \tag{34}$$

From (23) and (24),

$$\frac{a_{2c}b_{3c}}{a_{3c}b_{2c}} > 1. \tag{35}$$

Assuming the energy efficiency of the WPT system is larger than 50%, substituting (25) into (26) yields

$$\sqrt{ab} < 0.5c. \tag{36}$$

Using the condition of $\eta_{3c}^{\max} > \eta_{2c}^{\max}$, compared with (27) and (28), we obtain

$$\sqrt{a_{2c}b_{2c}} > \sqrt{a_{3c}b_{3c}}. \tag{37}$$

Using (36) and (37), the following inequality can be derived

$$\frac{4\sqrt{a_{3c}b_{3c}} + \frac{c^2}{\sqrt{a_{3c}b_{3c}}} + 4c}{4\sqrt{a_{2c}b_{2c}} + \frac{c^2}{\sqrt{a_{2c}b_{2c}}} + 4c} > 1. \tag{38}$$

Substituting (35) and (38) into (34) yields

$$\left.\left(\frac{\partial^2 \eta_{2c}}{\partial R_L^2} > \frac{\partial^2 \eta_{3c}}{\partial R_L^2}\right)\right|_{\eta=\eta^{\max}}. \tag{39}$$

Equation (39) indicates that the energy efficiency of the two-coil structure decreases faster than that of the three-coil system when the load resistance deviates from its optimal value. Fig. 6 illustrates the conclusions above. Both derivatives of the energy efficiency decrease very fast when R_L is small. When R_L increases, the rate of decrease of the derivatives becomes smaller. After crossing zero, the decreasing speeds become smaller and finally tend to zero again. When the derivatives of the energy efficiency cross zero, the systems achieve their maximum efficiency. At this point, the red curve (two-coil structure) clearly decreases faster than the pink curve (three-coil structure) and, therefore, the top area of the energy efficiency curve of the three-coil structure obtains better stiffness against load variations than that of the two-coil system. Because most systems operate around the maximum efficiency point, the above analysis represents the main characteristics of the system's stiffness.

D. Misalignment

Coil misalignments is likely unavoidable and, therefore, the efficiency and transfer power impact of the misalignment has been theoretically analyzed and experimentally tested [33], [39]–[42]. The system design considerations of the misalignment tolerance have been discussed in two-coil and four-coil systems [33], [39], but the deterioration of the EMF emission caused by misalignment and the misalignment effects on the three-coil system have not been fully addressed. The magnetic field leakage is approximately proportional to the input current of the system, which can be calculated from the input

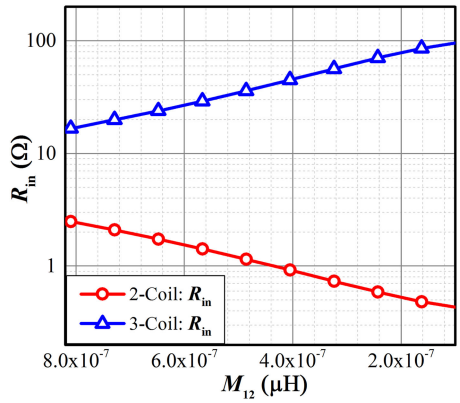

Fig. 7. Simulation results of the input impedance variations with mutual inductance

impedance. When the transmitter coil and the receiving coil are misaligned, the mutual inductance between the two coils reduces. From Table II, a decrease in M_{12} leads to a decreased input impedance of the two-coil system, and the opposite leads to an increased input impedance in the three-coil system. The simulation results of the input impedance variation with the mutual inductance are shown in Fig. 7, where a decrease in the x-axis values (M_{12}) corresponds to an increase in the coil misalignments. The current variations in the two structures with the coil misalignments can also be calculated from the circuit model. The current of the transmitter coil for the two-coil system is

$$\mathbf{I}_1^{2c} = \frac{\mathbf{U}_s}{\left(R_s + R_1 + \frac{\omega_0^2 M_{12}^2}{R_2 + R_L}\right)}. \tag{40}$$

When M_{12} decreases, $\mathbf{I}_1$ will increase. If there is no valid receiving coil placed near the transmitter coil, the source current will increase to

$$\mathbf{I}_1^{\infty_{2c}} = \frac{\mathbf{U}_s}{(R_s + R_1)}. \tag{41}$$

Because R_s and R_1 are small, $\mathbf{I}_1^{\infty_{2c}}$ is a very large value. The current of the receiving coil can be expressed as

$$\left|\mathbf{I}_1^{2c}\right| = \frac{|\mathbf{U}_s|}{\frac{R_s + R_1}{\omega_0 M_{12}} + \omega_0 M_{12}}. \tag{42}$$

Therefore, if $\omega_0 M_{12}$ is sufficiently large, then when the misalignment increases, the current of the receiving coil increases at the beginning and, then, will tend to zero. The current of the source coil for the three-coil system is

$$\mathbf{I}_0^{3c} = \frac{\mathbf{U}_s}{\left(R_s + \frac{\omega_0^2 M_{01}^2 (R_2 + R_L)}{R_1 (R_2 + R_L) + \omega_0^2 M_{12}^2}\right)}. \tag{43}$$

When M_{12} decreases, $\mathbf{I}_0$ will decrease. If there is no valid receiving coil placed near the transmitter coil, then the current of the source coil will decrease to

$$\mathbf{I}_0^{\infty_{3c}} = \frac{\mathbf{U}_s}{\left(R_s + \frac{\omega_0^2 M_{01}^2}{R_1}\right)}. \tag{44}$$

From (19), $\mathbf{I}_0^{\infty_{3c}}$ is much smaller than $\mathbf{I}_1^{\infty_{2c}}$. Substituting (43) into (13), the current of the transmitter coil for the three-coil system can be expressed as

$$\left|\mathbf{I}_1^{3c}\right| = \frac{|\mathbf{U}_s|}{K_{12} R_s + \omega_0 M_{01}} \tag{45}$$

where, K_{12} is defined as

$$K_{12} = \frac{\left|\mathbf{I}_0^{3c}\right|}{\left|\mathbf{I}_1^{3c}\right|} = \frac{R_1 (R_2 + R_L) + \omega_0^2 M_{12}^2}{\omega_0 M_{01} (R_2 + R_L)}. \tag{46}$$

$\left|\mathbf{I}_1^{3c}\right|$ also increases when M_{12} decreases, but the increase in $\left|\mathbf{I}_1^{3c}\right|$ is very slow. Because K_{12} must be smaller than 1 to reduce the equivalent source resistance and R_s is also small, from (45), $\left|\mathbf{I}_1^{3c}\right|$ is dominated by $\omega_0 M_{01}$. Therefore, $|\mathbf{I}_1|$ is approximately constant when M_{12} varies. The maximum value of $\left|\mathbf{I}_1^{3c}\right|$ is

$$|\mathbf{I}_1^{\infty_{3c}}| = \frac{|\mathbf{U}_s|}{\frac{R_1 R_s}{\omega_0 M_{01}} + \omega_0 M_{01}} \simeq \frac{|\mathbf{U}_s|}{\omega_0 M_{01}}. \tag{47}$$

Additionally, based on the assumption of (19), $|\mathbf{I}_1^{\infty_{3c}}|$ is much smaller than $|\mathbf{I}_1^{\infty_{2c}}|$. The current of the receiving coil can be expressed as

$$\left|\mathbf{I}_2^{3c}\right| = \frac{|\mathbf{U}_s|\, \omega_0^2 M_{01} M_{12}}{(R_2 + R_L)(R_s R_1 + \omega_0^2 M_{01}^2) + \omega_0^2 M_{12}^2 Rs}. \tag{48}$$

From this equation, if M_{12} is sufficiently large, the current of the receiving coil will also increase and then decrease. However, because the output power always decreases with the input power and the load is constant, the current of the receiving coil for the three-coil structure will always decrease and will tend to zero. This result means that in most applications, the current of the receiving coil will not increase when the misalignment increases because R_s is small and the term with R_s in (48) can be neglected.

The physical background of the above discussion is clear. For the two-coil structure, when $M_{12} = 0$, the transmitter coil is a pure resistive circuit at resonance frequency. Because the system is designed with very low resistance, the source current becomes very large. For the three-coil structure, on the one hand, when M_{12} decreases, the equivalent load of the transmitter coil will decrease. On the other hand, decreased M_{12} leads to an increase in the input impedance and a decrease in the source current I_0 and, therefore, the source of the transmitter coil $j\omega_0 M_{01} I_0$ will also decrease. Because both the load and source will decrease, the increase in $\left|\mathbf{I}_1^{3c}\right|$ is very slow and is approximately constant. When M_{12} tends to zero, the source current is approximately zero, and thus, the voltage drop on the resistor is approximately zero. Then, the voltage equation in the source loop is

$$\mathbf{U}_s = j\omega_0 M_{01} I_1. \tag{49}$$

This equation is the same as (47), which means that when the misalignment is very large, the circuit is purely inductive, and the energy in the inductor stops the increase in the current of the transmitter coil. Accordingly, without additional current control strategies, compared with the two-coil system, the three-coil system has the significant advantage of reducing the current stress of each coil, and therefore, it can also suppress the EMF emission that is caused by misalignments.

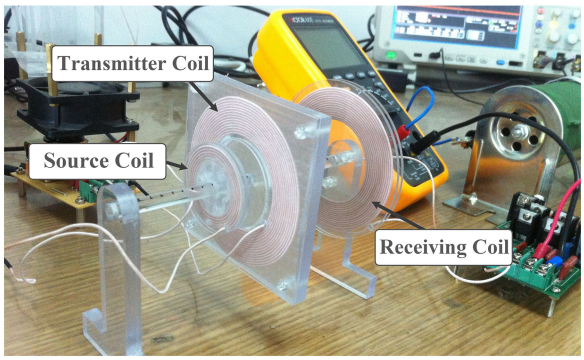

(a)

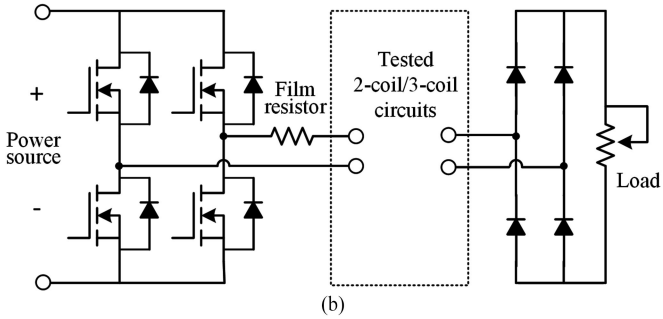

(b)

Fig. 8. Experimental setup. (a) Tested coils. (b) Topology of the test circuit.

IV. Results and Discussion

The experimental setup is shown in Fig. 8. Two 76-mm diameter closely wound circular coils (44-mm inner diameter) are used as the transmitter coil and receiving coil with a power transfer distance of $d_{12} = 62$ mm. A 36-mm diameter closely wound circular coil (24-mm inner diameter) is used as the source coil with an adjustable distance to the source coil. A Litz wire of 119 0.07 mm is used to fabricate the three coils. The parameters of the coils are shown in Table III. A KIKUSUI PAN110-10A is used as the power source. To understand the effect of internal resistance, an additional 0.2 Ω power film resistor is series connected in the source loop. An H-bridge inverter circuit is designed with four N-channel power MOSFETs of IRF3205, and four Schottky diodes of DSS25 are used in the full bridge rectifier circuit. Because it is inefficient to convert power at frequencies above the MHz level using state-of-the art power electronics devices [1] and the power transfer distance will be significantly limited for low resonant frequencies, the switching frequency of our experimental system is selected to be 684 kHz. The efficiency is measured by the output power divided by the supplied power. The output power and supplied power are obtained by the measured dc voltages and the dc currents in the circuit.

A comparison of the efficiency between the two- and three-coil systems is shown in Fig. 9. In this experiment, the dc output voltage is maintained at 8 V by adjusting the power source, and therefore, the nonlinear effects of the constant voltage drop of the diodes are equal for the two structures. The load resistance is adjusted from a small value to 20 Ω. For the three-coil system, d_{01} is set to zero. The simulation results are calculated using the expressions in Table III, and the equivalent resistances of the losses from the inverter and rectifier are included in R_s and R_2,

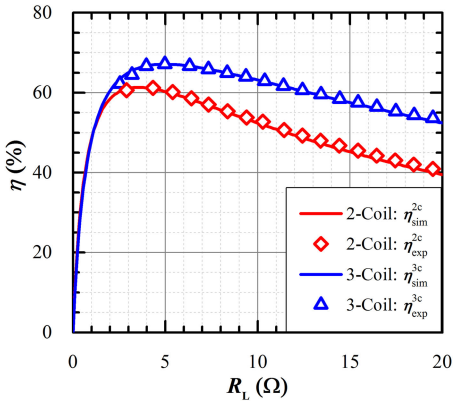

Fig. 9. Measured and simulated energy efficiencies of the three-coil and two-coil systems under different loading conditions.

respectively. The value of the ESR of the rectifier varies with the output power, which is assumed to be constant in our simulation and it could cause errors of the simulation results. However, because the load impedance is large, the errors are small; and because the output voltages are adjusted to the same value, the errors will not affect the efficiency comparison of the two structures. In Fig. 9, the measured and simulated energy efficiencies are well matched under different loading conditions, which verifies the circuit model proposed in Section II. Comparing the efficiency of the two- and three-coil structures, the maximum energy efficiency of the three-coil system is much higher than that of the two-coil system. This finding arises because in reference to (30), $M_{01}R_2/M_{12}R_1$ of this experimental prototype is approximately 3.7 and, thus, the maximum efficiency of the three-coil system shows significant benefit over that of the two coil system. We neglected R_0 in our simulation, which should lead to slight overestimation of the simulated energy efficiency of the three-coil structure. However, the simulation results match with the experimental results very well, which shows the feasibility of our assumption. Because R_0 is series connected with R_s (including the equivalent resistance of the inverter), a small increase of R_s can be assumed. Because R_s is converted to be very small to the transmitter coil by the source coil, especially when M_{01} is large, R_0 is of less importance. The stiffness of the energy efficiency against the load variation is verified using the same simulation and experimental results, but it is plotted differently, as shown in Fig. 10. In this figure, the x-axis represents the load deviation from the optimal value, and the y-axis represents the efficiency decline from the maximum point. The results show that the energy efficiency of the three-coil system decreases more slowly on both the left and right side than its two-coil counterpart and, therefore, the energy stiffness comparison of the two structures is experimentally verified.

As discussed in Section III, inequality (30) describes the condition for which the maximum energy efficiency of the three-coil system is larger than that of the two-coil system. In our experiments, M_{01} is selected to be adjusted to evaluate the efficiency relationship of the two structures. The adjustment of M_{01} is realized by changing d_{01}, and the maximum energy efficiencies for different values of d_{01} are recorded. M_{01} for different

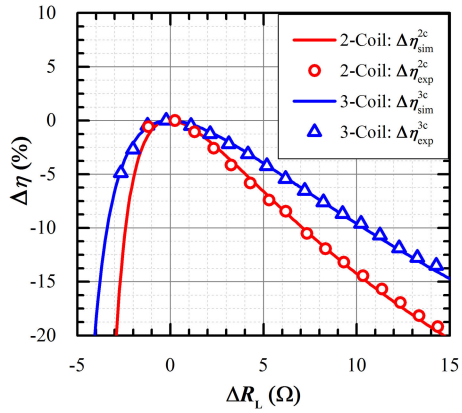

Fig. 10. Measured and simulated efficiency degradation with load variations.

TABLE IV
MUTUAL INDUCTANCES BETWEEN THE SOURCE COIL AND TRANSMITTER COIL

d_{01} (mm)	0	2	4	6	8	10	12	14
M_{01} (μH)	1.50	1.47	1.41	1.32	1.22	1.11	1.01	0.92
d_{01} (mm)	16	18	20	22	24	26	28	30
M_{01} (μH)	0.83	0.75	0.67	0.60	0.54	0.49	0.44	0.40

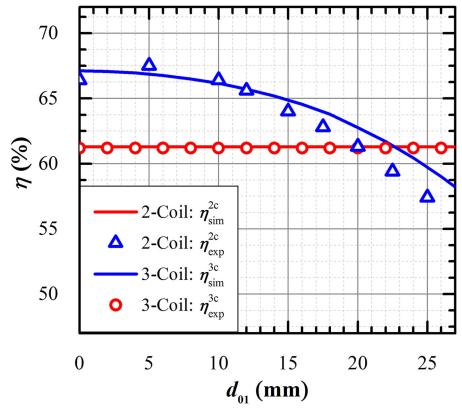

Fig. 11. Measured and simulated maximum energy efficiencies of the three-coil and two-coil systems for different d_{01}.

values of d_{01} in the simulation are calculated by the finite-element analysis (FEA) software ANSYS, and the calculated values for M_{01} are shown in Table IV. The experimental and simulation results are shown in Fig. 11. Because the maximum energy efficiency of the two-coil system has no relationship with M_{01}, it is denoted as a straight line. In Fig. 11, the energy efficiency decreases when d_{01} decreases, and when d_{01} is greater than 20 mm, the energy efficiency of the three-coil system begins to be lower than that of the two-coil system. Using the parameters in Tables III and IV, the critical condition of inequality (30) is $d_{01} = 22$ mm, therefore, the condition of inequality (30) is experimentally confirmed. Note that there are some differences between the measured and simulated results when d_{01} is large. This circumstance occurs because the induced voltage of the receiving coil decreases when d_{01} increases, which causes the nonlinear losses from the rectifier to become significant. However, the trends of the measured and simulated results match well, and a large value for d_{01} is not used in practical applications.

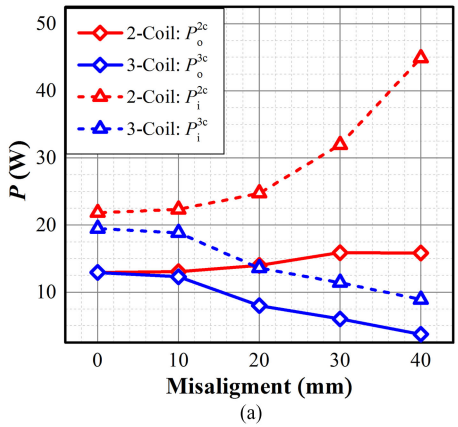

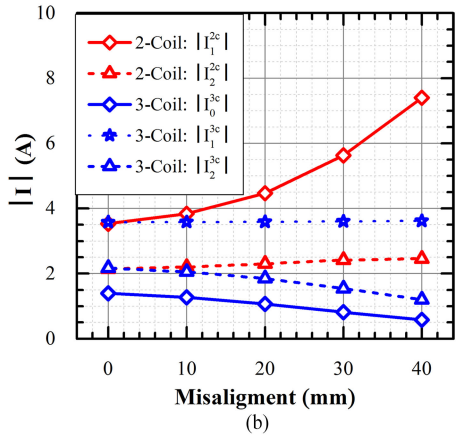

Fig. 12. Measured results under different misalignment conditions. (a) Transfer powers. (b) Currents(calculated).

To evaluate the effect of misalignment, the receiving coil is laterally misaligned from 0 to 40 mm. In this experiment, the misalignment is adjusted to 0 mm first, the dc output voltages of the two structures are adjusted to 8 V, and the output powers are both 12.9 W. Then, with the supply voltage maintained constant, the output voltage and output power vary with the misalignments. The experimental results under different misalignments are shown in Fig. 12(a). Consistent with previously discussed results, the input power of the two-coil system increases with the misalignment and achieves 44.9 W when the misalignment is 40 mm. In contrast, the input power of the three-coil system decreases with the misalignment and reduced to 8.9 W when the misalignment is 40 mm. Additionally, when the misalignment is 40 mm, the energy efficiency of the two-coil system is reduced to 35%, while its counterpart is 43%. These results show that the energy efficiency stiffness against the coil misalignments is also improved by the three-coil structure. Limited by our experimental resources, the current variations and the EMF emission of the coils that are caused by misalignment cannot be directly measured and, therefore, the currents are calculated based on the experimental measurements, and then, imported into the FEA models to simulate the induced magnetic fields.

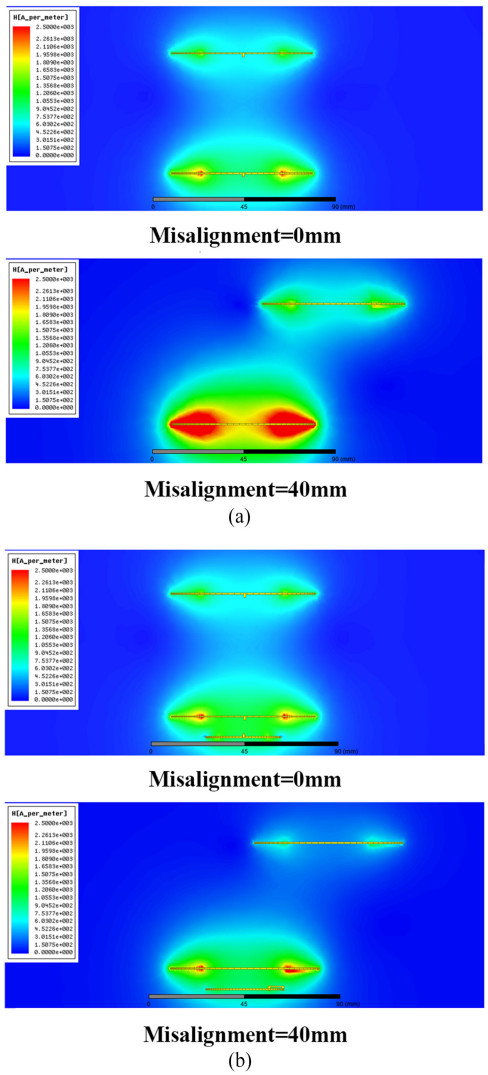

Fig. 13. Magnetic field of the three-coil and two-coil systems under different misalignment conditions. (a) Two-coil system. (b) Three-coil system.

ANSYS is used for the FEA simulation. The currents of the coils are shown in Fig. 12(b), and the FEA results are shown in Fig. 13. The calculated currents agree with our analysis very well. I_1^{3c} maintained at 3.8 A while I_1^{2c} increases very quickly when the misalignment increases. I_0^{3c} and I_2^{3c} both decrease, but I_2^{2c} increases. However, from our analysis, I_2^{2c} will decrease if the misalignment further increases. Apparently, the currents of the three-coil structure are suppressed and the induced magnetic fields show similar results. When the misalignments are 0 mm, the magnetic fields of the two systems are similar. However, when the misalignment is 40 mm, the EMF emission of the two-coil system is significant, while that of the three-coil system is suppressed. Although there is no experimental validation of the simulation results in Fig. 13, the experimentally measured powers clearly show the physical fundamentals of our conclusion, and the FEA results can be seen as an illustration of the EMF emission from the currents. In this scenario, the output powers of the two structures are adjusted to the same value as at the beginning for comparison. Otherwise, if the same supply voltages are used for comparison, then the EMF emission of the two-coil structure will be even larger. The reason is that considering the calculated input impedances in Fig. 4, if the supply voltages of the two structures are the same, then the power level of the two-coil structure will be much larger; thus, the EMF emission will increase proportionally.

V. Discussion and Conclusion

In this paper, the two- and three-coil WPT systems are theoretically analyzed and compared based on circuit theory. Simplified models of the two- and three-coil systems are proposed to evaluate the benefits of the three-coil structure. With the simplified models, the differences between the two- and three-coil structures become intuitive. The key advantages of the three-coil system, including the maximum energy efficiency, the energy efficiency stiffness against load variations and the reduced EMF emission induced by the coil misalignments are analyzed and proven. Simulation and experimental results are provided to confirm the analytical results.

A maximum energy efficiency comparison is the basis of the comparison of the two structures, and therefore, a simple condition is proposed to give a boundary of the maximum energy efficiency for the three-coil system that is larger than that for the two-coil system. This condition indicates that the source coil should be placed close to the transmitter coil and the three-coil structure obtained is especially advantageous when the transmitter coil and receiving coil are weakly coupled. Additionally, the ESRs of the transmitter coil and receiving coil are also important factors, especially when accounting for the power electronics losses. It is proven that the energy efficiency of the three-coil system decreases more slowly when the load resistance deviates from the optimal value, and therefore, the three-coil system exhibits better energy efficiency stiffness against load variations around the optimal operating point. Finally, the EMF emission of the two structures that is induced by misalignment is discussed. For a constant voltage source supply, with the coil misalignments increasing, the currents of the two-coil system tend to be much larger than those of the three-coil system. As a result, when the coils are misaligned, the EMF emission will be significantly increased in the two-coil system but maintained or reduced in the three-coil system.

This paper provides a fundamental analysis to understand the effect of additional coil in WPT systems, which is simple and intrinsic. The method is not only applicable to the comparison of the two- and three-coil system, but it also expected be used for the design and optimization of other WPT systems with additional coils. For example, it can be used to find the optimal distance between the additional coil and primary coil for the multicoil structures and to find an optimal matching network (loops and variable capacitors) for the multiloop topologies as in [18]. It also can be used to evaluate alternative compensation networks for new WPT systems as in [43] and [44].

The modeling of the nonlinearity of power electronics in a WPT system is a very challenging issue. In this paper, we included power electronics losses as constant equivalent

resistance, and we reduce the effect of the nonlinearity by properly selecting the experimental conditions for comparison. However, introducing the nonlinearity of the power electronics into circuit models could extend the scope of this research and provide more accurate simulation results for WPT analysis. Our analysis focuses only on the weakly coupled WPT system operating at the resonant frequency, and M_{02} is neglected. However, when d_{12} decreases, the coupling effect of the source coil and receiving coil cannot be ignored, and the optimal frequency of the maximum system efficiency could shift away from the resonant frequency. Therefore, for mid- and short-range WPT, comparative analysis of the two- and three-coil structures while considering the coupling effect of the source coil and receiving coil and the variations in the operating frequency are also very interesting topics.

REFERENCES

[1] S. Li and C. Mi, "Wireless power transfer for electric vehicle applications," *IEEE J. Emerg. Sel. Topics Power Electron.*, vol. 3, no. 1, pp. 4–17, Mar. 2015.

[2] J. Deng, W. Li, T. Nguyen, S. Li, and C. Mi, "Compact and efficient bipolar coupler for wireless power chargers: Design and analysis," *IEEE Trans. Power Electron.*, vol. 30, no. 11, pp. 6130–6140, Nov. 2015.

[3] S. Li, W. Li, J. Deng, T. Nguyen, and C. Mi, "A double-sided LCC compensation network and its tuning method for wireless power transfer," *IEEE Trans. Veh. Technol.*, vol. 64, no. 6, pp. 2261–2273, Jun. 2015.

[4] G. Covic and J. Boys, "Inductive power transfer," *Proc. IEEE*, vol. 101, no. 6, pp. 1276–1289, Jun. 2013.

[5] S. Lee, B. Choi, and C. Rim, "Dynamics characterization of the inductive power transfer system for online electric vehicles by laplace phasor transform," *IEEE Trans. Power Electron.*, vol. 28, no. 12, pp. 5902–5909, Dec. 2013.

[6] H. Wu, A. Gilchrist, K. Sealy, P. Israelsen, and J. Muhs, "A review on inductive charging for electric vehicles," in *Proc. IEEE Int. Electric Mach. Drives Conf.*, May 2011, pp. 143–147.

[7] P. Riehl, A. Satyamoorthy, H. Akram, Y.-C. Yen, J.-C. Yang, B. Juan, C.-M. Lee, F.-C. Lin, V. Muratov, W. Plumb, and P. Tustin, "Wireless power systems for mobile devices supporting inductive and resonant operating modes," *IEEE Trans. Microw. Theory Techn.*, vol. 63, no. 3, pp. 780–790, Mar. 2015.

[8] J. Taylor, Z. N. Low, J. Casanova, and J. Lin, "A wireless power station for laptop computers," in *Proc. IEEE Radio Wireless Symp.*, Jan. 2010, pp. 625–628.

[9] S. Hui, W. Zhong, and C. Lee, "A critical review of recent progress in mid-range wireless power transfer," *IEEE Trans. Power Electron.*, vol. 29, no. 9, pp. 4500–4511, Sep. 2014.

[10] N. Inagaki, "Theory of image impedance matching for inductively coupled power transfer systems," *IEEE Trans. Microw. Theory Techn.*, vol. 62, no. 4, pp. 901–908, Apr. 2014.

[11] M. Dionigi, M. Mongiardo, and R. Perfetti, "Rigorous network and full-wave electromagnetic modeling of wireless power transfer links," *IEEE Trans. Microw. Theory Techn.*, vol. 63, no. 1, pp. 65–75, Jan. 2015.

[12] W. Zhong and S. Hui, "Maximum energy efficiency tracking for wireless power transfer systems," *IEEE Trans. Power Electron.*, vol. 30, no. 7, pp. 4025–4034, Jul. 2015.

[13] H. Li, J. Li, K. Wang, W. Chen, and X. Yang, "A maximum efficiency point tracking control scheme for wireless power transfer systems using magnetic resonant coupling," *IEEE Trans. Power Electron.*, vol. 30, no. 7, pp. 3998–4008, Jul. 2015.

[14] M. Fu, H. Yin, X. Zhu, and C. Ma, "Analysis and tracking of optimal load in wireless power transfer systems," *IEEE Trans. Power Electron.*, vol. 30, no. 7, pp. 3952–3963, Jul. 2015.

[15] M. Kato, T. Imura, and Y. Hori, "Study on maximize efficiency by secondary side control using dc-dc converter in wireless power transfer via magnetic resonant coupling," in *Proc. World Electr. Veh. Symp. Exhib.*, Nov. 2013, pp. 1–5.

[16] T. C. Beh, M. Kato, T. Imura, S. Oh, and Y. Hori, "Automated impedance matching system for robust wireless power transfer via magnetic resonance coupling," *IEEE Trans. Ind. Electron.*, vol. 60, no. 9, pp. 3689–3698, Sep. 2013.

[17] Y. Lim, H. Tang, S. Lim, and J. Park, "An adaptive impedance-matching network based on a novel capacitor matrix for wireless power transfer," *IEEE Trans. Power Electron.*, vol. 29, no. 8, pp. 4403–4413, Aug. 2014.

[18] J. Kim and J. Jeong, "Range-adaptive wireless power transfer using multiloop and tunable matching techniques," *IEEE Trans. Ind. Electron.*, vol. 62, no. 10, pp. 6233–6241, Oct. 2015.

[19] A. Sample, D. Meyer, and J. Smith, "Analysis, experimental results, and range adaptation of magnetically coupled resonators for wireless power transfer," *IEEE Trans. Ind. Electron.*, vol. 58, no. 2, pp. 544–554, Feb. 2011.

[20] B. Tierney and A. Grbic, "Design of self-matched planar loop resonators for wireless nonradiative power transfer," *IEEE Trans. Microw. Theory Techn.*, vol. 62, no. 4, pp. 909–919, Apr. 2014.

[21] C.-J. Chen, T.-H. Chu, C.-L. Lin, and Z.-C. Jou, "A study of loosely coupled coils for wireless power transfer," *IEEE Trans. Circuits Syst. II, Exp. Briefs*, vol. 57, no. 7, pp. 536–540, Jul. 2010.

[22] A. Kurs, A. Karalis, R. Moffatt, J. D. Joannopoulos, P. Fisher, and M. Soljačić, "Wireless power transfer via strongly coupled magnetic resonances," *Science*, vol. 317, no. 5834, pp. 83–86, 2007.

[23] F. Zhang, S. Hackworth, W. Fu, C. Li, Z. Mao, and M. Sun, "Relay effect of wireless power transfer using strongly coupled magnetic resonances," *IEEE Trans. Magn.*, vol. 47, no. 5, pp. 1478–1481, May 2011.

[24] C. K. Lee, W. Zhong, and S. Hui, "Effects of magnetic coupling of nonadjacent resonators on wireless power domino-resonator systems," *IEEE Trans. Power Electron.*, vol. 27, no. 4, pp. 1905–1916, Apr. 2012.

[25] W. Zhong, C. K. Lee, and S. Hui, "General analysis on the use of tesla's resonators in domino forms for wireless power transfer," *IEEE Trans. Ind. Electron.*, vol. 60, no. 1, pp. 261–270, Jan. 2013.

[26] D. Ahn and S. Hong, "A study on magnetic field repeater in wireless power transfer," *IEEE Trans. Ind. Electron.*, vol. 60, no. 1, pp. 360–371, Jan. 2013.

[27] A. Rajagopalan, A. RamRakhyani, D. Schurig, and G. Lazzi, "Improving power transfer efficiency of a short-range telemetry system using compact metamaterials," *IEEE Trans. Microw. Theory Techn.*, vol. 62, no. 4, pp. 947–955, Apr. 2014.

[28] M. Kiani, U.-M. Jow, and M. Ghovanloo, "Design and optimization of a 3-coil inductive link for efficient wireless power transmission," *IEEE Trans. Biomed. Circuits Syst.*, vol. 5, no. 6, pp. 579–591, Dec. 2011.

[29] J. Zhang, X. Yuan, and C. Wang, "A study of three-coil magnetically coupled resonators for wireless power transfer," in *Proc. IEEE Int. Wireless Symp.*, Mar. 2015, pp. 1–4.

[30] S. Moon, B.-C. Kim, S.-Y. Cho, C.-H. Ahn, and G.-W. Moon, "Analysis and design of a wireless power transfer system with an intermediate coil for high efficiency," *IEEE Trans. Ind. Electron.*, vol. 61, no. 11, pp. 5861–5870, Nov. 2014.

[31] Y. Zhang, T. Lu, and Z. Zhao, "Reducing the impact of source internal resistance by source coil in resonant wireless power transfer," in *Proc. IEEE Energy Convers. Congr. Expo.*, Sep. 2014, pp. 845–850.

[32] W. Zhong, C. Zhang, X. Liu, and S. Hui, "A methodology for making a three-coil wireless power transfer system more energy efficient than a two-coil counterpart for extended transfer distance," *IEEE Trans. Power Electron.*, vol. 30, no. 2, pp. 933–942, Feb. 2015.

[33] D. Kurschner, C. Rathge, and U. Jumar, "Design methodology for high efficient inductive power transfer systems with high coil positioning flexibility," *IEEE Trans. Ind. Electron.*, vol. 60, no. 1, pp. 372–381, Jan. 2013.

[34] D. Ahn and S. Hong, "Wireless power transfer resonance coupling amplification by load-modulation switching controller," *IEEE Trans. Ind. Electron.*, vol. 62, no. 2, pp. 898–909, Feb. 2015.

[35] M. Kiani and M. Ghovanloo, "The circuit theory behind coupled-mode magnetic resonance-based wireless power transmission," *IEEE Trans. Circuits Syst. I, Reg. Papers*, vol. 59, no. 9, pp. 2065–2074, Sep. 2012.

[36] T. Imura and Y. Hori, "Maximizing air gap and efficiency of magnetic resonant coupling for wireless power transfer using equivalent circuit and neumann formula," *IEEE Trans. Ind. Electron.*, vol. 58, no. 10, pp. 4746–4752, Oct. 2011.

[37] S. Cheon, Y.-H. Kim, S.-Y. Kang, M. L. Lee, J.-M. Lee, and T. Zyung, "Circuit-model-based analysis of a wireless energy-transfer system via coupled magnetic resonances," *IEEE Trans. Ind. Electron.*, vol. 58, no. 7, pp. 2906–2914, Jul. 2011.

[38] D. Ahn and S. Hong, "A transmitter or a receiver consisting of two strongly coupled resonators for enhanced resonant coupling in wireless power transfer," *IEEE Trans. Ind. Electron.*, vol. 61, no. 3, pp. 1193–1203, Mar. 2014.

[39] Q. Zhu, Y. Guo, L. Wang, C. Liao, and F. Li, "Improving the misalignment tolerance of wireless charging system by optimizing the compensate capacitor," *IEEE Trans. Ind. Electron.*, vol. 62, no. 8, pp. 4832–4836, Aug. 2015.
[40] Z. Dang and J. Qahouq, "Modeling and investigation of magnetic resonance coupled wireless power transfer system with lateral misalignment," in *Proc. 29th Annu. IEEE Appl. Power Electron. Conf. Expo.*, Mar. 2014, pp. 1317–1322.
[41] M. Q. Nguyen, Z. Hughes, P. Woods, Y.-S. Seo, S. Rao, and J.-C. Chiao, "Field distribution models of spiral coil for misalignment analysis in wireless power transfer systems," *IEEE Trans. Microw. Theory Techn.*, vol. 62, no. 4, pp. 920–930, Apr. 2014.
[42] Z. Yan, Y. Li, C. Zhang, and Q. Yang, "Influence factors analysis and improvement method on efficiency of wireless power transfer via coupled magnetic resonance," *IEEE Trans. Magn.*, vol. 50, no. 4, pp. 1–4, Apr. 2014.
[43] M. Budhia, J. T. Boys, G. A. Covic, and H. Chang-Yu, "Development of a single-sided flux magnetic coupler for electric vehicle IPT charging systems," *IEEE Trans. Ind. Electron.*, vol. 60, no. 1, pp. 318–328, Jan. 2013.
[44] L. Weihan, Z. Han, L. Siqi, D. Junjun, K. Tianze, and C. C. Mi, "Integrated LCC compensation topology for wireless charger in electric and plug-in electric vehicles," *IEEE Trans. Ind. Electron.*, vol. 62, no. 7, pp. 4215–4225, Jul. 2015.

Jian Zhang (S'15) was born in Chongqing, China, in 1989. He received the B.S. and M.S. degrees in thermal energy and power engineering from Jilin University, Changchun, China, in 2012 and 2015, respectively.

He is currently with United Automotive Electronic Systems Co. Ltd., Shanghai, China, as an Engineer. His research interests include wireless power transfer and design and optimization of high-power dc–dc converters for automotive applications.

Xinmei Yuan (M'13) received the B.S. and Ph.D. degrees in electrical engineering from Tsinghua University, Beijing, China, in 2004, and 2010, respectively.

From 2008 to 2009, he studied as a Visiting Student in the Department of Electrical and Computer Engineering, University of Wisconsin, Madison, WI, USA. He is currently an Associate Professor at the College of Automotive Engineering, Jilin University, Changchun, China. His research interests include power electronics and motor control, modeling and control of electric vehicles, and emission control of diesel engines.

Chuang Wang (S'15) was born in Xuzhou, China, in 1990. He received the B.S. degree in automotive engineering from Huaiyin Institute of Technology, Huaian, China. He is currently working toward the M.S. degree in thermal energy and power engineering at Jilin University, Changchun, China.

His research interests include wireless power transfer and microwave approaches for noncontact measurements.

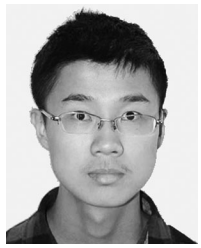

Yang He was born in Anhui, China, in 1994. He received the B.S. degree in thermal energy and power engineering from Jilin University, Changchun, China, in 2015, where he is currently working toward the M.S. degree in thermal energy and power engineering.

His current research interests include design and optimization of wireless systems for automotive applications.